Vol 18 No 1, January 2009
1674-1056/2009/18(01)/0149-08

Chinese Physics B

© 2009 Chin. Phys. Soc.
and IOP Publishing Ltd

Theoretical study of slowing supersonic CH_3F molecular beams using electrostatic Stark decelerator*

Deng Lian-Zhong(邓联忠), Fu Guang-Bin(符广彬), and Yin Jian-Ping(印建平)†

State Key Laboratory of Precision Spectroscopy, Department of Physics, East China Normal University, Shanghai 200062, *China*

(Received 14 April 2008; revised manuscript received 22 May 2008)

We have calculated the Stark effect of CH_3F molecules in external electrical fields, the rotational population of supersonic CH_3F molecules in different quantum states, and analyse the motion of weak-field-seeking CH_3F molecules in a state $|J = 1, KM = -1\rangle$ inside the electrical field of a Stark decelerator by using a simple analytical model. Three-dimensional Monte Carlo simulation is performed to simulate the dynamical slowing process of molecules through the decelerator, and the results are compared with those obtained from the analytical model, including the phase stability, slowing efficiency as well as the translational temperature of the slowed molecular packet. Our study shows that with a modest dipole moment (∼1.85 Debye) and a relatively slight molecular weight (∼34.03), CH_3F molecules in a state $|J = 1, KM = -1\rangle$ are a good candidate for slowing with electrostatic field. With high voltages of ±10 kV applied on the decelerator, molecules of 370 m/s can be brought to a standstill within 200 slowing stages.

Keywords: molecular beam, stark effect, stark decelerator
PACC: 3260S, 3510D, 4110D

1. Introduction

Manipulation and control of polar molecules based on the interaction of their electrical dipole moment with an electrical field (so-called Stark effect) has been an interesting subject in atomic and molecular physics.[1−7] Some polar molecules, such as CO,[8] ND_3,[9] OH,[10] YbF,[11] H_2CO,[12] SO_2[13] and NH,[14] have so far been successfully slowed using the so-called Stark decelerator, and its success has opened a new way to obtain cold molecules, which can be widely applied in the study of cold molecular spectroscopy,[15] measurement of fundamental physical constants,[16] study of cold molecular collision[17] and quantum computation based on electric dipole–dipole interactions,[18] and molecule scattering[19] and cold molecular chemistry, and so on. Therefore, it would be interesting and worthwhile to find some other new molecular species and demonstrate their possibility for Stark deceleration, even to study their dynamic behaviour inside the Stark decelerator, which can provide some theoretical basis for designing a desirable Stark decelerator.

In this paper, we propose a new molecular species (CH_3F) for slowing with time-varying electric field, the so-called Stark decelerator, and study the deceleration of a supersonic CH_3F molecular beam by Monte Carlo simulation. In Section 2, we calculate the stark shift of CH_3F molecules in external electrical fields and the rotational population of a supersonic CH_3F beam in different quantum states. In Section 3, we analyse the motion of weak-field-seeking molecules of state $|J = 1, KM = -1\rangle$ inside the electrical field of a decelerator by using a simple analytical model. In Section 4, we carry out three-dimensional (3D) Monte Carlo simulation of slowing CH_3F molecules in state $|J = 1, KM = -1\rangle$ with a decelerator of 150 electrical stages. Results from both theoretical model and 3D simulation are presented, including the phase stability, slowing efficiency as well as the translational temperature of the slowed molecular packet.

2. Stark shift of CH_3F and its rotational populations

As a symmetric-top molecule, CH_3F has a permanent dipole moment μ of 1.85 Debye along the

*Project supported by the National Natural Science Foundation of China (Grant Nos 10374029, 10434060 and 10674047), the National Key Basic Research and Development Program of China (Grant No 2006CB921604), and the Basic Key Program of Shanghai Municipality of China (Grant No 07JC14017), the Program for Changjiang Scholar and Innovative Research Team, and the Shanghai Leading Academic Discipline Project of China (Grant No B408).

†Corresponding author. E-mail: jpyin@phy.ecnu.edu.cn

C–F bond of the molecular symmetry axis with its rotational constants $A = 154.000\,\mathrm{GHz}$, $B = C = 25.536\,\mathrm{GHz}$.[20] Since we are only interested in the Stark shifts of the energy levels in an external electrical field, a rigid symmetric rotor can be regarded as a good approximation. The Stark interacting Hamiltonian operator can be expressed as

$$H_E = -\boldsymbol{\mu} \cdot \boldsymbol{E} = \mu\, E\, \Phi_{Zz}, \tag{1}$$

where E is the electric distribution, and Φ_{Zz} is the direction cosine of the molecular symmetry axis with respect to the direction of the external field. According to the first-order perturbation theory, the first-order Stark energy, which is the average of H_E over the unperturbed rotational states, is given by[21]

$$W^{(1)} = -\frac{\mu E K M}{J(J+1)}, \tag{2}$$

where J represents the total angular momentum number, K and M are the projections of J on the molecular symmetry axis and the external field, respectively. The second-order term of the Stark perturbation, which reflects the influences from neighbouring quantum states, can be expressed as[21]

$$W^{(2)} = \frac{\mu^2 E^2}{2hB}\left\{\frac{(J^2-K^2)(J^2-M^2)}{J^3(2J-1)(2J+1)} - \frac{\left[(J+1)^2-K^2\right]\left[(J+1)^2-M^2\right]}{(J+1)^3(2J+1)(2J+3)}\right\}, \tag{3}$$

where h is the Plank constant, and B is the rotational constant.

From Eqs.(2) and (3), we calculate the Stark shifts of the lowest rotational quantum states of CH_3F molecule in the external electric field E, and the results are depicted in Fig.1.

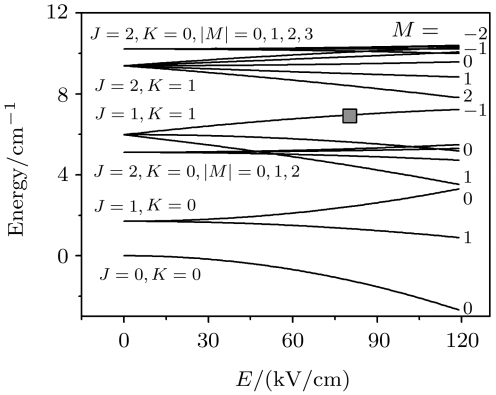


Fig.1. Stark shifts of the rotational energy levels of ground-state CH_3F molecules in an external electrical field E.

Since the first-order Stark shift $W^{(1)}$ is proportional to KM, and the second-order Stark shift $W^{(2)}$ is a function of both K^2 and M^2, so there is a degeneracy over KM for $K \neq 0$. For instance, the quantum states $|J=1,\ K=-1,\ M=1\rangle$ and $|J=1,\ K=1,\ M=-1\rangle$ are degenerate and are designated as $|J=1,\ KM=-1\rangle$. Fortunately, for Stark deceleration of polar molecules, it is the Stark energy (or shift) not the absolute energy of the quantum state that really counts, so the above approximation is totally reasonable. For quantum states with $K=0$, the first-order Stark shift is zero, and molecules will experience a quadratic Stark shift due to the second-order Stark effect, which decreases with the increase of J and is negligible for states with $J>1$. For states with $K>1$ they are rarely populated in a supersonic CH_3F beam with a low rotational temperature, which will be discussed below.

Under the conditions of thermal equilibrium the relative population of the different quantum states is given by Boltzmann distribution law and the degeneracy of the different states. For a supersonic molecular beam with a translational temperature of a few Kelvin, almost all molecules are populated in the vibrational and electronic ground state, and we only need to consider its rotational populations. We consider a supersonic CH_3F beam seeded in a Xe carrier gas with a rotational temperature of $\sim$5 K, and calculate the relative populations of the lowest weak-field-seeking rotational states $|J,K,M\rangle$, and the results, including the Stark shift W at $E = 90\,\mathrm{kV/cm}$ and their zero-field energy, are shown in Table 1. The different $|M|$ states with the same J and K quantum numbers are assumed to be equally populated in building Table 1. For quantum states with $K>1$, they contribute little to the total molecular population. For example, the relative population of the $|22-2\rangle$ state

Table 1. The relative populations of some lowest weak-field-seeking rotational states $|J,\ K,\ M\rangle$ of CH_3F molecules, including their zero-field energy and the Stark shift W at $E = 90\,\mathrm{kV/cm}$.

state	contribution/%	$E_{\mathrm{rot}}/\mathrm{cm}^{-1}$	W/cm^{-1}
1 0 0	12.5	1.70	0.92
2 0 0	3.1	5.11	0.22
1 1 −1	4.3	5.98	1.05
2 1 −1	1.0	9.39	0.50
2 1 −2	1.0	9.39	0.74
3 0 0	0.37	10.21	0.10
2 2 −2	0.005	22.24	1.74

is less than 0.005. It is clear from Table 1 that the quantum states with a higher population and a larger Stark shift are only $|J = 1, K = 0, M = 0\rangle$ and $|J = 1, KM = -1\rangle$. However, we can see from Fig.1 that the $|J = 1, K = 0, M = 0\rangle$ state has no first-order (i.e., linear) Stark effect, so we only focus our interest on the weak-field-seeking state of $|J = 1, KM = -1\rangle$ (marked with a square in Fig.1), which shows a relatively large linear Stark shift.

3. Motion of CH_3F molecules inside a decelerator

Schematic diagram of the whole electrostatic slowing system used in our discussion is shown in Fig.2. A skimmed CH_3F molecular beam first fly into a 50-mm-long hexapole, then enter into the 750-mm-long Stark decelerator. Molecules are counted at the

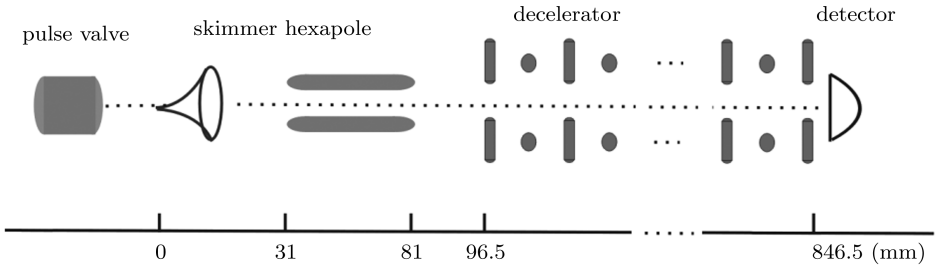


Fig.2. Schematic diagram of the whole electrostatic slowing system used in our discussion.

end of the decelerator. The hexapole, acting as a molecular lens, is composed of six 3-mm-diameter electrodes and applied a high voltage of ±8.0 kV. The decelerator, similar to those used by other groups,[1,3] is composed of 150 deceleration stages, and each stage consists of two 3-mm-diameter electrodes with a centre-to-centre distance of 5 mm, leaving a 2 mm opening for the propagation of the slowed molecular beam in the Z direction. Neighbouring deceleration stages are positioned alternately in X and Y directions and spaced with a centre-to-centre distance L of 5 mm.

For the sake of our convenient discussion, we will briefly summarize the working principle of a Stark decelerator as follows: when a polar molecule in a weak-field-seeking state moves in an increasing axial electric field generated by each deceleration stage, it experiences a positive and increased Stark potential. This increase in potential energy is compensated by its loss of kinetic energy. When the molecule arrives at some point in the axial electric field, the deceleration voltages are abruptly switched off, the potential energy of the molecule will be reduced almost to zero, and the molecule cannot regain its lost kinetic energy, so it will be slowed. When this deceleration process is repeated multi-times, the velocity of the molecule can be slowed even to zero.

To describe the longitudinal position of moving CH_3F molecules in the decelerating electric field a phase angle ϕ can be introduced, which is defined as $\phi = z\pi/L$, where L is the distance between the two adjacent decelerating stages, and z is the longitudinal position of the moving molecule in the Stark decelerator. Each decelerating stage is composed of a pair of electrodes. When the electric fields are being switched, a molecule at the midpoint of two adjacent stages is assigned a value of $\phi = 0°$, and molecules just in between the two electrodes of a pair, where the maximum electrical fields appear in the longitudinal direction, are assigned a value of $\phi = 90°$. Molecules that travel the same distance L between two adjacent electrical field switches lose the same amount of kinetic energy and are called synchronous molecules. Their phase and velocity are denoted as the equilibrium phase angle ϕ_0 and the equilibrium velocity v_0, respectively.

The lost kinetic energy of the synchronous molecules per stage can be well approximated by a Fourier series truncated at the second term[22]

$$\Delta K(\phi_0) = A_1 \sin(\phi_0) + A_3 \sin(3\phi_0). \tag{4}$$

The equation governing the motion of the nonsynchronous molecules relative to that of the synchronous molecules is given by

$$\frac{\mathrm{d}^2\Delta\phi}{\mathrm{d}t^2} + \frac{\pi}{mL^2}\{A_1[\sin(\phi) - \sin(\phi_0)] + A_3[\sin(3\phi) - \sin(3\phi_0)]\} = 0, \tag{5}$$

where $\Delta\phi = \phi - \phi_0$ is the instantaneous difference in phase of a nonsynchronous molecule relative to the

motion of a synchronous molecule, and m is the mass of the molecule. For CH_3F molecules in the $|J = 1, KM = -1\rangle$ state, we have $A_1 = 1.020\,\mathrm{cm}^{-1}$, and $A_3 = -0.028\,\mathrm{cm}^{-1}$ when high voltages of $\pm 10\,\mathrm{kV}$ are applied on the electrodes of the Stark decelerator. During our following discussion, the applied high voltages of $\pm 10\,\mathrm{kV}$ on the electrodes remain without specification, and the term containing coefficient A_3 in Eq.(5) is neglected for simplicity.

When the equilibrium phase angle ϕ_0 falls within the range of 0° and 90°, there exists a stable area in the phase space.[22,23] Molecules inside this "packet" will oscillate around the synchronous molecule and keep their original phase density during the process of slowing; while molecules outside this "packet" will not follow the synchronous molecule stably and spread randomly during the slowing process. Obviously, the upper limit of the phase angle corresponding to the phase stable area, denoted as $\phi^+_{\max}(\phi_0)$, is $\pi - \phi_0$. By the time of integration of Eq.(5) and using the boundary condition $\dot{\phi} = 0\Big|_{\phi=\phi^+_{\max}}$, we obtain

$$\dot{\phi}^2 = 2a_1(\cos\phi + \cos\phi_0 + (\phi + \phi_0 - \pi)\sin\phi_0), \quad (6)$$

where $a_1 = \dfrac{\pi}{mL^2}A_1$. By solving the transcendental equation $\dot{\phi} = 0$, we can obtain the lower limit $\phi^-_{\max}(\phi_0)$ of the phase stable area. Figure 3 shows the dependence of $\phi^+_{\max}$ and $\phi^-_{\max}$ on the equilibrium phase angle ϕ_0 for CH_3F molecules in the $|J = 1, KM = -1\rangle$ state. When $\phi_0 = 60°$, we have $\phi^+_{\max} = 120°$ and $\phi^-_{\max} \approx 29°$.

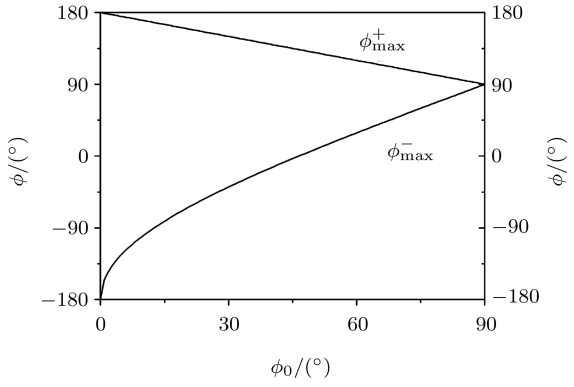


Fig.3. The dependence of the upper and lower limits ($\phi^+_{\max}$ and $\phi^-_{\max}$) of the phase angle inside the phase stable zone on the synchronous phase angle ϕ_0 for CH_3F molecules in the $|J = 1, KM = -1\rangle$ state.

The maximum velocity deviation of the non-synchronous molecules inside the phase stable area relative to the synchronous molecule, $\Delta v_{\max}(\phi_0) = |v - v_0|$, can be obtained from Eq.(6) at the position $\phi = \phi_0$, and is give by

$$\Delta v_{\max}(\phi_0) = 2\sqrt{\frac{A_1}{m\pi}\left(\cos\phi_0 - \left(\phi_0 - \frac{\pi}{2}\sin\phi_0\right)\right)}. \quad (7)$$

Figure 4 shows $\Delta v_{\max}$ as a function of ϕ_0 for CH_3F molecules in the $|J = 1, KM = -1\rangle$ state. When ϕ_0 changes from 0° to 90°, $\Delta v_{\max}$ decreases from 21.5 m/s to 0. Now, we have enough information to show the phase stable area of CH_3F molecules concerned. Figure 5 shows the separatrix of the phase stable area of CH_3F molecules in state $|J = 1, KM = -1\rangle$ in the decelerator with ϕ_0 taking values of 0°, 15°, 30°, 45°, 60° and 75°, respectively. It is clear from Fig.5 that with the increase of ϕ_0, the phase stable area inside the separatrix reduces rapidly. This shows that fewer molecules can be obtained inside the slowed molecular 'packet' with the increase of ϕ_0.

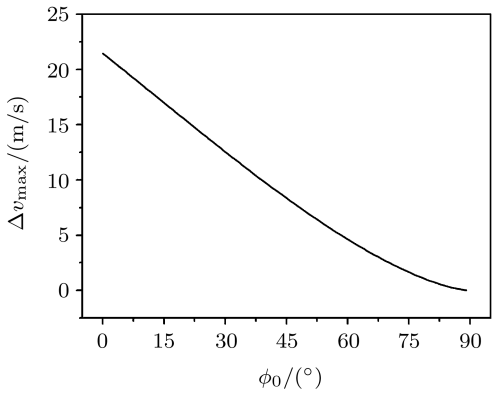


Fig.4. The dependence of the maximum velocity deviation $\Delta v_{\max}(\phi_0) = |v - v_0|$ of molecules inside the phase stable zone relative to the synchronous molecule on the synchronous phase angle ϕ_0.

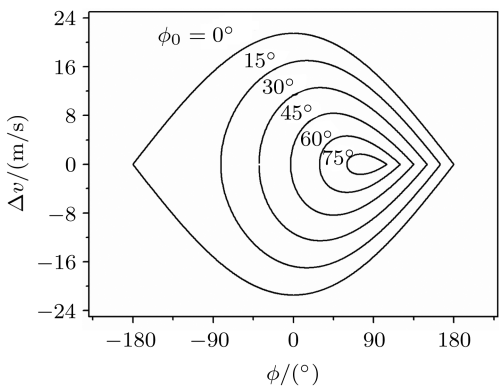


Fig.5. Separatrix of phase stable zone for CH_3F molecules in state $|J = 1, KM = -1\rangle$ with $\phi_0 = 0°$, 15°, 30°, 45°, 60° and 75°, respectively.

The transverse motion of the molecules inside the decelerator is rather complicated. For the sake of

simplicity, we assume that the molecules move in a quadratic transverse potential well. In this case, we can introduce an average force $\bar{F}_x(\phi)$ (or $\bar{F}_y(\phi)$ on the molecules in the longitudinal phase stable area, and assume $\bar{F}_x(\phi) = -\bar{K}_x(\phi)x$ (or $\bar{F}_y(\phi) = -\dot{K}_y(\phi)y$) near the molecular beam axis. Since the molecules are focused only in one direction for each slowing stage, $\bar{K}_x$ (or $\bar{K}_y$) has to be averaged over a distance of $2L$[22]

$$\bar{K}_{x,y}(\phi) = \frac{1}{2L}\int_{\phi L/\pi}^{(\phi+2\pi)L/\pi} K_{x,y}(z)\mathrm{d}z. \qquad (8)$$

From Eq.(8), we numerically calculate the transverse force constant for CH_3F molecules in the $|J=1, KM=-1\rangle$ state inside the Stark decelerator, and the corresponding result is shown by the solid line in Fig.6. The dotted line represents the maximum depth of the transverse potential well, i.e., the well depth at the transverse position 1 mm away from the beam axis. When $\phi = 60°$, the maximum depth is $\sim 0.015\,\mathrm{cm}^{-1}$. This shows that the molecules with a transverse velocity of lower than ~ 3.2 m/s can be trapped during the whole deceleration process.

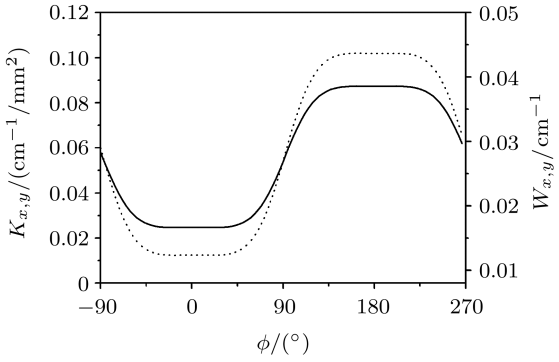


Fig.6. The average transverse force constant inside the decelerator as a function of phase angle ϕ for CH_3F molecules in state $|J=1, KM=-1\rangle$ (solid line). The dotted line represents the maximum depth of the transverse potential well.

4. Monte Carlo simulation and results

To demonstrate the possibility of Stark deceleration for the CH_3F molecules, we perform Monte Carlo simulation for its dynamic slowing process. In our simulation, the decelerated CH_3F beam in the $|J=1, KM=-1\rangle$ state has a FWHM (full width at half maximum) of 80 m/s centred at 370 m/s, which is obtainable by supersonically expanding binary mixture of CH_3F and Xe at room temperature. The physics under our simulation is simple and classical: Due to Stark effect, moving molecules in electrostatic fields experience a dipole gradient force. All molecules are taken as particles which observe Newton's dynamics. Based on our numerically solved electric fields inside both the hexapole and the Stark decelerator, a time sequence is first obtained by letting a synchronous molecule of a certain initial speed pass through the whole electrostatic slowing system (from the skimmer to the end of the decelerator, as shown in Fig.2) at a selected phase angle ϕ_0. Then, by the same time sequence molecules different in velocities and positions in three dimensions (x, y, and z) fly through the whole slowing system, and are recorded with their time of arrival at the exit of the decelerator.

Firstly, we simulate the time of flight (TOF) signals of the CH_3F molecules arriving at the end of the decelerator of 150 stages for the phase angle $\phi_0 = 0°, 15°, 30°, 45°, 60°$ and $75°$. The corresponding results are shown in Fig.7, from which we can find that with the increase of the phase angle ϕ_0, more kinetic energy is extracted from the slowed molecules, and a molecular packet coming out with a lower velocity is obtained from the decelerator. For instance, when $\phi_0 = 60°$ CH_3F molecules with an initial velocity of 370 m/s can be slowed to 214 m/s after passing off 150 stages.

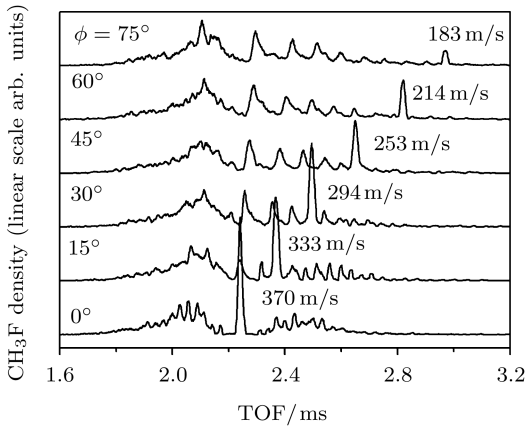


Fig.7. Simulated time of flight (TOF) signals of CH_3F molecules in state $|J=1, KM=-1\rangle$ at the outlet of the decelerator for various synchronous phase angle ϕ_0.

Secondly, we study the dependence of the lost kinetic energy after each stage on the phase angle ϕ_0, and the result obtained is shown in Fig.8, where the solid squares are results from 3D Monte Carlo simulation, and the solid line is theoretically calculated result from Eq.(4). It can be seen from Fig.8 that with the increase of the phase angle, the lost kinetic energy per

stage will be first increased almost linearly and then approach gradually to a saturated value. For $\phi_0 = 0°$, 15°, 30°, 45°, 60°, 75° and 90°, the lost kinetic energy ΔK per stage from 3D Monte Carlo simulation are $0\,\mathrm{cm}^{-1}$, $0.240\,\mathrm{cm}^{-1}$, $0.474\,\mathrm{cm}^{-1}$, $0.686\,\mathrm{cm}^{-1}$, $0.860\,\mathrm{cm}^{-1}$, $0.976\,\mathrm{cm}^{-1}$ and $1.017\,\mathrm{cm}^{-1}$ with their theoretical counterparts being $0\,\mathrm{cm}^{-1}$, $0.240\,\mathrm{cm}^{-1}$, $0.475\,\mathrm{cm}^{-1}$, $0.686\,\mathrm{cm}^{-1}$, $0.861\,\mathrm{cm}^{-1}$, $0.980\,\mathrm{cm}^{-1}$ and $1.020\,\mathrm{cm}^{-1}$. As we can see, simulated results are in good agreement with the theoretically predicted ones. For a fixed phase angle ϕ_0, the final speed of the slowed molecular packet depends on the number of the decelerating stages used. To bring the molecules with an initial kinetic energy $E_{\mathrm{K}0}$ to a standstill, the number of the decelerating stages needed is given by $N = E_{\mathrm{K}0}/\Delta K(\phi_0)$. For example, when $\phi_0 = 75°$, to bring CH_3F molecules with an initial velocity of 370 m/s ($E_{\mathrm{K}0} \sim 196\,\mathrm{cm}^{-1}$) to a standstill, the number of decelerating stages required is about 200.

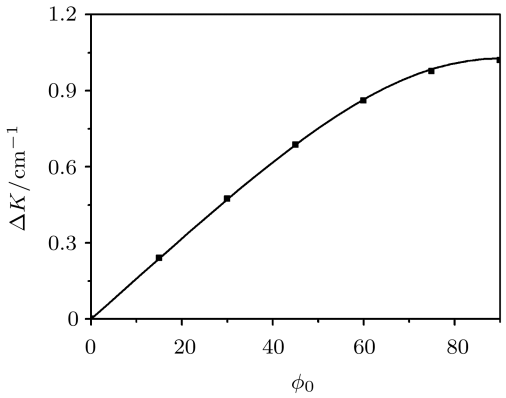


Fig.8. Kinetic energy loss per stage ΔK as a function of the synchronous phase angle ϕ_0. The solid line is the theoretically calculated result from Eq.(4), and the solid squares are the results from 3D Monte Carlo simulation for $\phi_0 = 0°$, 15°, 30°, 45°, 60°, 75° and 90°.

To verify this, we study the dependence of the final velocity of the slowed molecular packet on the number of the decelerating stages, and the results are shown in Fig.9. We can see from Fig.9 that when the number of the decelerating stages is increased from 0 to 200, the mean velocity of the molecular packet is slowed from 370 m/s to zero.

Afterwards, we come to study the phase space distribution of the slowed CH_3F molecular packet exiting the decelerator. In Fig.10 the initial phase space distribution of CH_3F molecules entering the decelerator during our simulation is shown in grey dots. The molecular beam has a FWHM of 80 m/s in the longitudinal speed and a FWHM of 20 mm in the longitudinal

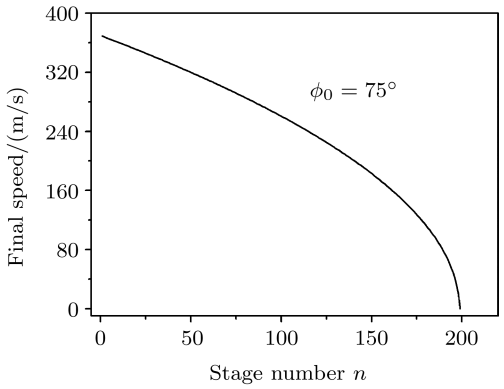


Fig.9. Final speed of the slowed molecular packet as a function of the slowing stage number n with slowing time sequence designed for initial molecular velocity of 370m/s ($E_{\mathrm{K}}0 \sim 196\,\mathrm{cm}^{-1}$) and $\phi_0 = 75°$.

space, as shown in Fig.10 by dotted lines. The solid lines correspond to separatrix of the phase stable zones derived from Eq.(6) for $\phi_0 = 0°$, 30° and 60°. The phase space distribution of the slowed CH_3F molecular packet after 150 slowing stages from 3D simulation is analysed. Shown in Fig.11 in grey dots are phase space distributions of the slowed molecular packets for $\phi_0 = 45°$, 60° and 75°. For comparison, the separatrixes of their corresponding phase stable zones obtained from Eq.(6) are shown in solid lines as well. Below the phase stable diagrams are the TOF signals of the slowed molecular packets arriving at the end of the decelerator. Similar results are obtained for other values of ϕ_0 and omitted here to avoid redundancy. As we can see, with the increase of phase angle ϕ_0, a slowed molecular packet arrives at the end of the decelerator at a later time due to its lower velocity, but the number of molecules inside the slowed packet decreases dramatically due to the reduction of the phase stable zone.

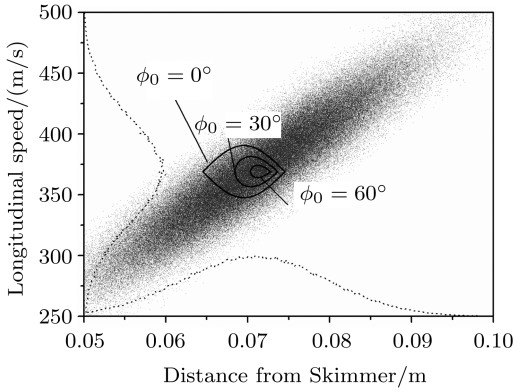


Fig.10. Initial phase space of CH_3F molecules entering the decelerator. The molecular beam has a longitudinal velocity FWHM of 80m/s and a FWHM of 20 mm in the longitudinal space, as shown by the dotted lines.

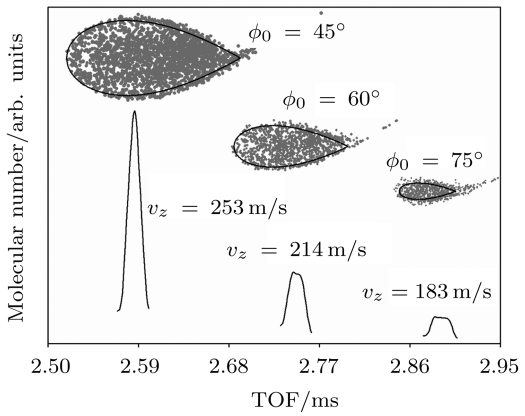


Fig.11. Phase space distribution of CH_3F molecules inside the slowed packet after 150 slowing stages for $\phi_0 = 45°$, 60° and 75°, together with the separatrix of the phase stable zone obtained from Eq.(6). Below the phase stable diagrams are the TOF signals of the slowed molecular packets arriving at the end of the decelerator.

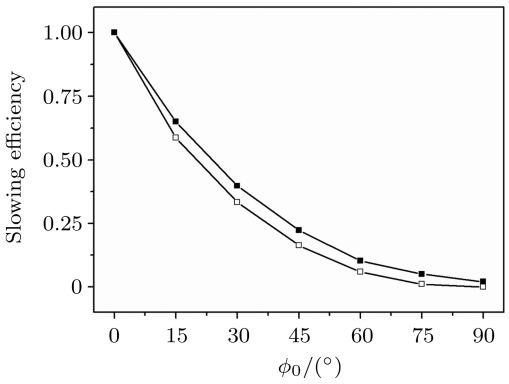


Fig.12. Slowing efficiency η of CH_3F molecules as a function of the synchronous phase angle ϕ_0. The solid squares represent results from 3D simulations while the blank squares represent results from a rough estimation based on the calculated area of the phase stable zone. The solid lines are just for eye-guiding.

Finally, we study the dependences of the slowing efficiency and the translational temperature of the slowed molecular packet on the phase angle ϕ_0. The slowing efficiency η of the decelerator is defined as the ratio of the number of molecules in the slowed molecular packet output from the decelerator to that of molecules entering the decelerator. Provided that molecules occupy the whole phase stable zone and fill it uniformly when being loaded into the decelerator (as shown in Fig.10), we can roughly estimate the slowing efficiency by calculating the area of the phase stable zone for a selected phase angle ϕ_0. For simplicity, we ignore any difference in transverse confinement of molecules for different phase angles. Corresponding results are shown in blank squares in Fig.12 for various phase angles with solid squares representing results from 3D Monte Carlo simulations. All results in Fig.12 are normalized to that of $\phi_0 = 0°$. For $\phi_0 = 0°$, 15°, 30°, 45°, 60°, 75° and 90°, slowing efficiencies from 3D Monte Carlo simulation are ∼100%, ∼65%, ∼40%, ∼22%, ∼10%, ∼3% and ∼1% with their counterparts from a rough estimation based on the calculated area of the phase stable zone being ∼100%, ∼58%, ∼33%, ∼17%, ∼6%, ∼1% and 0, respectively. As we can see, results from Monte Carlo simulation are slightly larger than those from the rough estimation above. Particularly, for $\phi_0 = 90°$, the result from the analytical model indicates that the area of the phase stable zone should be zero, which means no phase stable area exists, but we do find a very small slowed molecular packet during our 3D simulation. In fact, with the increase of phase angle the transverse confinement of molecules in the decelerator gets increasingly strong, as can be found in Fig.6, which is we believe partly responsible for the difference between the slowing efficiencies obtained from the above two methods. The translational temperature of the slowed molecular packet exiting the decelerator is also analysed. For instance, when $\phi_0 = 60°$, simulation result indicates that the mean longitudinal velocity of the slowed molecular packet is ∼214m/s with a FWHM of ∼5.6m/s, corresponding to a translational temperature of ∼60mK, while the calculated translational temperature from Eq.(7) is ∼50mK. Temperatures of slowed molecular packets for other phase angles are studied similarly and corresponding results are shown in Fig.13 with solid squares and blank squares representing the results from 3D simulation and calculation based on Eq.(7), respectively. For $\phi_0 = 0°$, 15°, 30°,

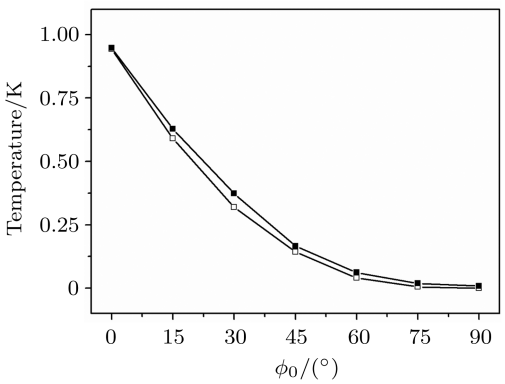


Fig.13. Translational temperature of the slowed molecular packet as a function of phase angle ϕ_0. The solid squares represent results from 3D simulations and the blank squares are results obtained from Eq.(7).

45°, 60° and 75°, translational temperatures of slowed molecular packets from 3D Monte Carlo simulation are ∼947, ∼628, ∼374, ∼166, ∼60, and ∼10 mK with their theoretical counterparts from Eq.(7) being ∼943, ∼590, ∼320, ∼143, ∼50, and ∼6 mK respectively. As we can see, with the increase of the phase angle ϕ_0, the translational temperature of the slowed molecular packet will be lowered, and the simulated results are consistent with the calculated ones in spite of their discrepancies in absolute values.

5. Conclusion

We have calculated the stark potential of CH_3F molecules in external electrical fields and the rotational population of different quantum states in a supersonic CH_3F beams, and studied the dynamic motion of the CH_3F molecules in the weak-field-seeking $|J = 1,\ KM = -1\rangle$ state inside the electrostatic field of a Stark decelerator by using both a theoretical model and the three-dimensional Monte Carlo simulation. Our study shows that the CH_3F molecules in the $|J = 1,\ KM = -1\rangle$ state can be efficiently slowed to a very low even zero velocity. With a high voltage of ±10 kV applied on the decelerator electrodes and a reasonable phase angle $\phi = 75°$, the kinetic energy loss per stage is as large as $\sim 0.98\,\mathrm{cm}^{-1}$, and the molecules with a velocity of ∼370 m/s can be slowed down to a standstill within 200 decelerating stages. We have also analysed the phase stability of CH_3F molecules in the $|J = 1,\ KM = -1\rangle$ state, the corresponding slowing efficiency, and the translational temperature of the slowed molecular packet.

In principle, the stronger the used electrostatic field is, the greater the Stark shift of CH_3F molecules will be, and then the better the Stark deceleration effect is. Unfortunately, with the increase of the electric field the Stark shifted energy level of the $|J = 1,\ KM = -1\rangle$ state will cross those of neighbouring rotational states, which may exhibit a negative Stark shift (see Fig.1), even result in a nonadiabatic transition between them[24] and a loss of the CH_3F molecules concerned. During our simulation, however, the CH_3F molecules never experience an electrostatic field greater than 120kV/cm, so the above problem cannot occur.

Acknowledgments

We acknowledge generous help from Dr Eric R. Hudson and Professor Jun Ye in JILA in building our simulation code.

References

[1] Jongma R T, Rasing T and Meijer G 1995 *J. Chem. Phys.* **102** 1925
[2] Harland P W, Hu W P and Vallance C 1999 *Phys. Rev.* A **60** 3138
[3] Loesch H J and Scheel B 2000 *Phys. Rev. Lett.* **85** 2709
[4] Junglen T, Rieger T, Pinkse P W H and Rempe G 2004 *Phys. Rev. Lett.* **92** 223001
[5] Xia Y, Yin Y, Chen H, Deng L and Yin J 2008 *Phys. Rev. Lett.* **100** 043003
[6] Deng L, Xia Y and Yin J 2007 *Chin. Phys.* **16** 707
[7] Deng L and Yin J 2007 *Opt. Lett.* **32** 1695
[8] Bethlem H L, Berden G and Meijer G 1999 *Phys. Rev. Lett.* **83** 1558
[9] Bethlem H L, Berden G, Crompvoets F M H, Jongma R T, van Roij A J A and Meijer G 2000 *Nature* **406** 491
[10] Bochinski J R, Hudson E R, Lewandowski H J, Meijer G and Ye J 2003 *Phys. Rev. Lett.* **91** 243001
[11] Hudson J J, Sauer B E, Tarbutt M R and Hinds E A 2001 *Phys. Rev. Lett.* **89** 023003
[12] Hudson E R, Ticknor C, Sawyer B C, Taatjes C A, Lewandowski H J, Bochinski J R, Bohn J L and Ye J 2006 *Phys. Rev.* A **73** 063404
[13] Jung S, Tiemann E and Lisdat C 2006 *Phys. Rev.* A **74** 040701
[14] van de Meerakker S Y T, Labazan I, Hoekstra S, Kupper J and Meijer G 2006 *J. Phys.* B **39** S1077
[15] van Veldhoven J, Kupper J, Bethlem H L, Sartakov B, van Roij A J A and Meijer G 2004 *Eur. Phys. J.* D **31** 337
[16] Chengalur J N and Kanekar N 2003 *Phys. Rev. Lett.* **91** 241302
[17] Avdeenkov A V and Bohn J L 2002 *Phys. Rev.* A **66** 052718
[18] DeMille D 2002 *Phys. Rev. Lett.* **88** 067901
[19] Bohn J L 2000 *Phys. Rev.* A **66** 040702
[20] Larkin D M and Gordy W 1963 *J. Chem. Phys.* **38** 2329
[21] Gordy W and Cook R L 1984 *Microwave Molecular Spectra* (3rd Edition) (New York: John Wiley & Sons) p452
[22] Bethlem H L, Crompvoets F M H, Jongma R T, van de Meerakker S Y T and Meijer G 2002 *Phys. Rev.* A **65** 53416
[23] Gubbels K, Meijer G and Friedrich B 2006 *Phys. Rev.* A **73** 063406
[24] Schwettmann A, Franklin J, Overstreet K R and Shaffer J P 2005 *J. Chem. Phys.* **123** 194305